Chemistry of Iron Oxophlorins. 2. Oxidation of the Iron(III) Octaethyloxophlorin Dimer and Observation of Stepwise, Two-Electron Oxidation of the Oxophlorin Macrocycle

Alan L. Balch,*,† Lechosław Latos-Grażyński,‡ Bruce C. Noll,† Ludmiła Szterenberg,‡ and Edward P. Zovinka†

Contribution from the Departments of Chemistry, University of California, Davis, California 95616, and University of Wrocław, Wrocław, Poland

Received July 29, 1993®

Abstract: The oxidation of iron oxophlorin (*meso*-hydroxyporphyrin) complexes has been studied in order to understand the basic chemical reactivity which may contribute to the heme destruction that is catalyzed by heme oxygenase. Reaction of the iron(III) octaethyloxophlorin dimer $[Fe^{III}(OEPO)]_2$ with molecular bromine results in the formation of two new, highly oxidized complexes, $BrFe^{III}(OEPO^{\cdot})$ and $Br_2Fe^{III}(OEPOx)$ (where $OEPO^{\cdot}$ and OEPOx are the octaethyloxophlorin dianion radical and the oxidized octaethyloxophlorin monoanion, respectively), in which the experimental data suggest that it is the ligand rather than the iron that has undergone oxidation. $BrFe^{III}(OEPO^{\cdot})\cdot CHCl_3$ has been crystallized and subjected to a structure determination by X-ray crystallography. The iron is five-coordinate with structural parameters consistent with the presence of high-spin ($S = {}^5/_2$) Fe(III). The magnetic moment (4.9(2) μ_B at 23 °C) for $BrFe^{III}(OEPO^{\cdot})$ suggests that there is strong antiferromagnetic coupling between the iron and ligand spins. $Br_2Fe^{III}(OEPOx)$ has a magnetic moment of 5.7(2) μ_B at 23 °C and displays an EPR spectrum typical of an axially symmetric, high-spin iron(III) complex with hyperfine splitting due to the two axial ligands clearly resolved. Electronic absorption and ^1H NMR spectra for both oxidation products are presented and interpreted. The ^1H NMR spectrum of $BrFe^{III}(OEPO^{\cdot})$ with some methylene resonances with upfield hyperfine shifts and others with downfield hyperfine shifts and very large downfield meso shifts indicates that this complex possesses a remarkable electronic structure.

Introduction

Heme oxygenase catabolizes unwanted heme by converting it to the green pigment biliverdin. This is subsequently reduced by biliverdin reductase to form bilirubin which can be excreted. Scheme I shows a widely accepted path for the conversion of heme to biliverdin. The first step utilizes molecular oxygen to effect meso hydroxylation of the heme to form an iron oxophlorin complex.[4] This subsequently undergoes further oxidation that results in the formation of verdoheme and the conversion of the oxygenated meso carbon into carbon monoxide which is removed through the lungs. While there has been considerable speculation on the mechanism of the first step,[1-3,5,6] the hydroxylation of heme, very little has been offered regarding the second step,[7,8] which culminates in carbon monoxide loss.

Iron complexes of oxophlorins have received relatively little systematic study, and there have been no reports of crystallographic characterization of iron oxophlorin complexes. Iron does form a dimeric complex, **1**, $[Fe^{III}(OEPO)]_2$, with the symmetric oxophlorin octaethyloxophlorin (abbreviations: P, generic porphyrin dianion; OEP, octaethylporphyrin dianion; OEPO, octaethyloxophlorin trianion; TPP, tetraphenylporphyrin dianion; and py, pyridine). This dimer, which shows weak antiferromagnetic coupling between the iron ions, has been studied by a range of spectroscopic techniques.[5-10] Recently, the structure of the related indium complex $[In^{III}(OEPO)]_2$ has been determined by X-ray crystallography.[11] This study confirms earlier conclusions (based on molecular mechanics calculations) about the shape of such a dimer.[10] Complex **1** undergoes cleavage by

Scheme I. Heme Oxygenation

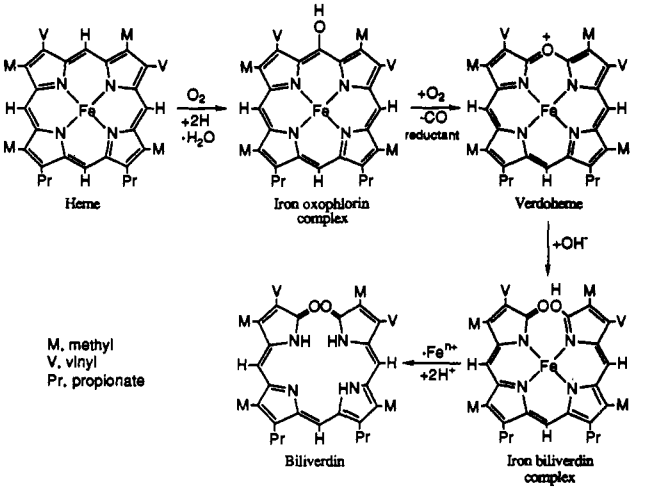

† University of California, Davis.
‡ University of Wrocław.
® Abstract published in *Advance ACS Abstracts,* November 15, 1993.

(1) Bissell, D. M. Bile Pigments and Jaundice. In *Liver: Normal Function and Disease*; Ostrow, J. D., Ed.; Marcel Decker, Inc.: New York, 1986; Vol. 4, p 133.
(2) Schmid, R.; McDonagh, A. F. In *The Porphyrins*; Dolphin, D., Ed.; Academic Press: New York, 1979; Vol. 6, p 258.
(3) O'Carra, P. In *Porphyrins and Metalloporphyrins*; Smith, K. M., Ed.; Elsevier: New York, 1975; p 123.
(4) Yoshida, T.; Naguchi, M.; Kikuchi, G.; Sano, S. *J. Biochem.* **1981**, *90*, 125.
(5) Brown, S. B. *Biochem. J.* **1976**, *159*, 23.
(6) Olmstead, M. M.; Cheng, R.-J.; Balch, A. L. *Inorg. Chem.* **1982**, *21*, 4143.
(7) Rajanands, V.; Brown, S. B. *Tetrahedron* **1983**, *39*, 1927.
(8) Masuoka, N.; Itano, H. A. *Biochemistry* **1987**, *26*, 3672.
(9) Bonnett, R.; Dimsdale, M. J. *J. Chem. Soc., Perkin Trans.* **1972**, 2540.
(10) Balch, A. L.; Latos-Grażyński, L.; Noll, B. C.; Olmstead, M. M.; Zovinka, E. P. *Inorg. Chem.* **1992**, *31*, 2248.
(11) Balch, A. L.; Noll, B. C.; Olmstead, M. M.; Reid, S. M. *J. Chem. Soc., Chem. Commun.* **1993**, 1088.

0002-7863/93/1515-11846$04.00/0

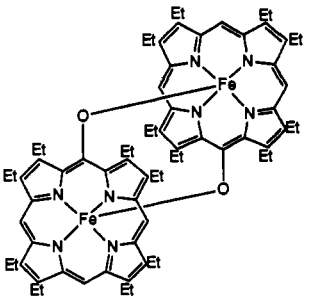

1, $\{Fe^{III}(OEPO)\}_2$

Brønsted acids (HX) to form high-spin, five-coordinate complexes, $XFe^{III}(OEPOH)$, in which the meso oxygen is protonated.[10] It also undergoes cleavage by Lewis bases (B = isocyanides, pyridine) to form six-coordinate complexes, $B_2Fe(OEPO)$,[8] whose electronic structures have received considerable attention and are somewhat controversial.[8,12,13]

On the basis of current knowledge about porphyrin and oxophlorin chemistry, oxidation of the iron oxophlorin complexes could be expected to lead to one of several outcomes: oxidation of either the iron or the macrocyclic unit to form a high-valent species or oxidative attack upon the oxophlorin ring to initiate ring cleavage. The electronic structures of high-valent iron porphyrin complexes are regulated to a considerable degree by the nature of the axial ligation. Complexes in which oxidation of the iron to the iron(IV) state has been documented include examples with a single axial oxo ligand (where the well-known ferryl unit $(Fe^{IV}{=}O)^{+2}$ is present),[14] an axial phenyl ligand,[15] or two axial methoxide ligands.[16] Oxidation of the porphyrin ligand to form a π-radical has been observed with axial chloride, bromide, perchlorate, and imidazole ligands.[17-27] Removal of two electrons from iron(III) porphyrins generates species with an even higher oxidation level. The best characterized of these are formulated as containing both the ferryl unit $(Fe^{IV}{=}O)^{2+}$ and a porphyrin radical.[13d,28-31]

Previous work has shown that the oxophlorin ligand and its complexes are more readily oxidized than their porphyrin counterparts.[32-34] Consideration of the electronic structure of the oxophlorin ligand suggests that three oxidation states are possible. These include the fully reduced form, the trianion OEPO; a one-electron oxidation product, the radical $OEPO^{\cdot}$; and a two-electron oxidation product, the monoanion OEPOx. The

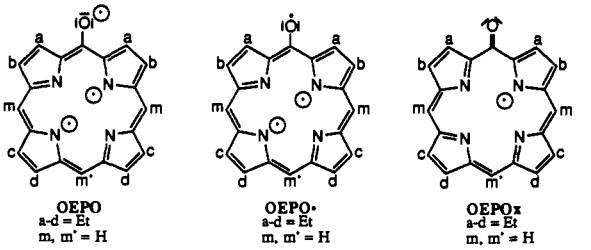

oxidation of complexes of octaethyloxophlorin to form stable radicals has been previously documented. Thus, treatment of $(py)Zn^{II}(OEPOH{\cdots}py)$ with dioxygen in pyridine solution produces the green, air-stable radical $[(py)Zn^{II}(OEPO^{\cdot})](py)$.[35] Similarly, $Ni^{II}(OEPOH)$ is converted to $(py)_2Ni^{II}(OEPO^{\cdot})$ upon treatment with dioxygen or diiodine in pyridine solution.[36] Both of these radicals have been isolated in crystalline form and characterized by X-ray crystallography. However, $(py)_2Ni^{II}(OEPO^{\cdot})$ undergoes dimerization through C–C bond formation between meso carbon atoms to form $Ni_2(OEPO)_2$ when it is crystallized from chloroform solution.[37]

Heme catabolism is a process that is highly dependent on the presence of iron within the macrocycle. Free protoporphyrin is not oxidized by heme oxygenase. Some of its metal complexes, particularly zinc(II) protoporphyrin, act as competitive inhibitors of this enzyme.[38] For that reason, it is particularly important to establish the reactivity of iron complexes in the various stages of heme degradation. Here, we describe studies of the chemical oxidation of **1**.

Results

Spectroscopic Characterization of $BrFe^{III}(OEPO^{\cdot})$. Solutions of $[Fe^{III}(OEPO)]_2$ in noncoordinating solvents (chloroform, dichloromethane, toluene) are unreactive toward dioxygen. They are, however, oxidized by dibromine and dichlorine. The oxidation products produced by dibromine oxidation have been isolated and characterized. Similar reactions with dichlorine have been monitored by ^1H NMR spectroscopy. Spectra indicative of the formation of similar products were obtained, but the dichlorine oxidation products were not isolated.

Addition of bromine to $[Fe^{III}(OEPO)]_2$ in a 1:1 molar ratio cleaves the dimer to produce $BrFe^{III}(OEPO^{\cdot})$, **2**, which has been

(12) Sano, S.; Sugiura, Y.; Maeda, Y.; Ogawa, S.; Morishima, I. *J. Am. Chem. Soc.* **1981**, *103*, 2888. Morishima, I.; Fujii, H.; Shiro, Y.; Sano, S. *J. Am. Chem. Soc.* **1986**, *108*, 3858.
(13) Balch, A. L.; Noll, B. C.; Reid, S. M., Zovinka, E. P. *Inorg. Chem.* **1993**, *32*, 2610.
(14) (a) Chin, D. H.; Balch, A. L.; La Mar, G. N. *J. Am. Chem. Soc.* **1980**, *102*, 1446. (b) Chin, D. H.; La Mar, G. N.; Balch, A. L. *J. Am. Chem. Soc.* **1980**, *102*, 5945. (c) La Mar, G. N.; de Ropp, J. S.; Latos-Grażyński, L.; Balch, A. L.; Johnson, R. B.; Smith, K. M.; Parish, D. W.; Cheng, R. J. *J. Am. Chem. Soc.* **1983**, *105*, 782. (d) Penner-Hahn, J. E.; McMurray, T. J.; Latos-Grażyński, L.; Renner, M.; Eble, K. S.; Davis, I. M.; Balch, A. L.; Groves, J. T.; Dawson, J. H.; Hodgson, K. O. *J. Biol. Chem.* **1983**, *258*, 12761. (e) Balch, A. L.; La Mar, G. N.; Latos-Grażyński, L.; Renner, M. W.; Tanabal, V. *J. Am. Chem. Soc.* **1985**, *107*, 3003.
(15) Balch, A. L.; Renner, M. W. *J. Am. Chem. Soc.* **1986**, *108*, 2603. Lancon, D.; Cocolios, P.; Guilard, R.; Kadish, K. M. *J. Am. Chem. Soc.* **1984**, *106*, 4472.
(16) Groves, J. T.; Quinn, R.; McMurry, T. J.; Nakamura, M.; Lang, G.; Boso, B. *J. Am. Chem. Soc.* **1985**, *107*, 354.
(17) Phillippi, M. A.; Shimomura, E. T.; Goff, H. M. *Inorg. Chem.* **1981**, *20*, 1322.
(18) Gans, P.; Marchon, J.-C.; Reed, C. A.; Regnard, J.-R. *Nouv. J. Chim.* **1981**, 203.
(19) Shimomura, E. T.; Phillippi, M. A.; Goff, H. M.; Scholz, W. F.; Reed, C. A. *J. Am. Chem. Soc.* **1981**, *103*, 6778.
(20) Phillippi, M. A.; Goff, H. A. *J. Am. Chem. Soc.* **1982**, *104*, 6026.
(21) Scholz, W. F.; Reed, C. A.; Lee, Y. J.; Scheidt, W. R.; Lang, G. *J. Am. Chem. Soc.* **1982**, *104*, 6791.
(22) Buisson, G.; Deronzier, A.; Duee, E.; Gans, P.; Marchon, J.-C.; Regnard, J.-R. *J. Am. Chem. Soc.* **1982**, *104*, 6793.
(23) Gans, P.; Buisson, G.; Duee, E.; Marchon, J.-C.; Erler, B. S.; Scholz, W. F.; Reed, C. A. *J. Am. Chem. Soc.* **1986**, *108*, 1223.
(24) Lang, G.; Boso, G.; Erler, B. S.; Reed, C. A. *J. Chem. Phys.* **1986**, *84*, 2998.
(25) Erler, B. S.; Scholz, W. F.; Lee, Y. J.; Scheidt, W. R.; Reed, C. A. *J. Am. Chem. Soc.* **1987**, *109*, 2644.
(26) Nakashima, S.; Ohya-Nishiguchi, M.; Hirota, N.; Fujii, H.; Morishima, I. *Inorg. Chem.* **1990**, *29*, 5207.
(27) Scheidt, W. R.; Song, H.; Haller, K. J.; Safo, M. K.; Orosz, R. D.; Reed, C. A.; Debrunner, P. G.; Schulz, C. E. *Inorg. Chem.* **1992**, *31*, 939.
(28) Groves, J. T.; Haushalter, R. C.; Nakamura, M.; Nemo, T. E.; Evans, B. J. *J. Am. Chem. Soc.* **1981**, *103*, 2884.
(29) Boso, B.; Lang, G.; McMurry, T. J.; Groves, J. T. *J. Chem. Phys.* **1983**, *79*, 1122.
(30) Hickman, D. L.; Nanthakumar, A.; Goff, H. M. *J. Am. Chem. Soc.* **1988**, *110*, 6384.
(31) Gold, A.; Jayaraj, K.; Doppelt, P.; Weiss, R.; Chottard, G.; Bill, E.; Ding, X.; Trautwein, A. X. *J. Am. Chem. Soc.* **1988**, *110*, 5756.
(32) Bonnett, R.; Dimsdale, M. J.; Sales, K. D. *J. Chem. Soc., Chem. Commun.* **1970**, 962.
(33) Fuhrhop, J.-H.; Besecke, S.; Subramanian, J. *J. Chem. Soc., Chem. Commun.* **1973**, 1.
(34) Fuhrhop, J.-H.; Besecke, S.; Subramanian, J.; Mengersen, C.; Riesner, D. *J. Am. Chem. Soc.* **1975**, *97*, 7141.
(35) Balch, A. L.; Noll, B. C.; Zovinka, E. P. *J. Am. Chem. Soc.* **1992**, *114*, 3380.
(36) Balch, A. L.; Noll, B. C.; Phillips, S. L.; Reid, S. M.; Zovinka, E. P. *Inorg. Chem.* **1993**, *32*, in press.
(37) Balch, A. L.; Noll, B. C.; Reid, S. M.; Zovinka, E. P. *J. Am. Chem Soc.* **1993**, *115*, 2531.
(38) Drummond, G. S.; Kappas, A. *Proc. Natl. Acad. Sci. U.S.A.* **1981**, *78*, 6466.

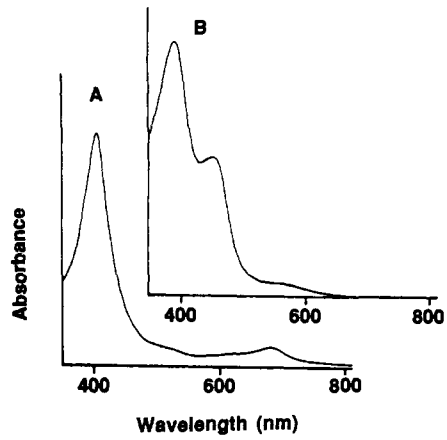

Figure 1. Electronic absorption spectra of chloroform solutions of: (A) $BrFe^{III}(OEPO^{\cdot})$, λ_{max}, nm (ϵ, $M^{-1}cm^{-1}$) 406 (9.6×10^4), 514 (7.9×10^3), 683 (8.0×10^3) and (B) $Br_2Fe^{III}(OEPOx)$, 393 (6.0×10^4), 449 (3.0×10^4), 574 (3.7×10^3).

Table I. ^1H NMR Data for Iron Octaethyloxophlorin Complexes

compound	T (°C)	chemical shifts (ppm) meso	methylene	methyl
$BrFe^{III}(OEPO^{\cdot})$, **2**	25	344.2, 232.2	65.5, 61.5, 59.3, 58.5, 2.30, −3.0, −15.1, −21.0	4.80,[b] 4.60, 2.10
$ClFe^{III}(OEPO^{\cdot})$	25	345.0, 232.7	61.8, 60.9, 58.2, 56.5, −2.2, −4.4, −17.0, −23.9	[c]
$BrFe^{III}$(Etio I $O^{\cdot}$)	25	346.5, 232.8	62.8, 61.8, 59.7, 58.6, [c], −3.3, −17.1, −19.3	95.2,[d] 94.1,[d] −14.7,[d] −51.9,[d] 5.2,[e] 4.7,[e] 4.0,[e] 3.6[e]
$Br_2Fe^{III}(OEPOx)$, **3**	24	35.4, 21.8	56.9, 49.9, 44.8, 33.4	6.97, 6.79, 6.14, 6.03
$Cl_2Fe^{III}(OEPOx)$	25	23.9, 12.2	48.4, 42.6, 38.3, 20.0	
Br_2Fe^{III}(Etio I Ox)	25	36.8, 23.6	58.3, 50.5, 45.9, 34.7	82.7,[d] 67.0,[d] 62.8,[d] 43.2[d]
$[Fe^{III}(OEPO)]_2$, **1**[a]	28	−98.4, −28.0	39.1, 37.1, 33.6, 31.8, 30.0, 28.8, 23.2, 18.0	5.2, 4.4, 4.1, −1.4
$BrFe^{III}(OEPOH)$[a]	25	−71.7, −66.3	53.4, 49.6, 46.2, 44.3, 43.6	8.7, 7.4, 7.1, 1.5

[a] Data from ref 10. [b] Intensity double that of other methyl resonances. [c] Obscured by diamagnetic impurities at *ca.* 4–2 ppm. [d] Methyl on pyrrole. [e] β-Methyl of ethyl groups. [f] β-Methyl in diamagnetic region and not identified.

isolated as red plates. The electronic absorption spectrum of the complex is shown in trace A, Figure 1.

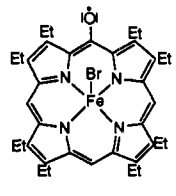

2, $BrFe^{III}(OEPO^{\cdot})$

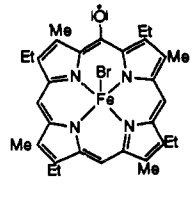

2a, $BrFe^{III}$(Etio I $O^{\cdot}$)

^1H NMR data for $BrFe^{III}(OEPO^{\cdot})$ and related complexes are given in Table I. Figure 2 shows the ^1H NMR spectrum of the complex in chloroform-*d* at 24 °C. Individual resonances are readily identified on the basis of their intensity and the fact that, in general, the meso protons, which are closer to the iron than the methylene or methyl protons, give the broadest resonances.[39,40] The two types of meso protons show remarkably large downfield shifts. Eight methylene resonances are observed. Four are near 60 ppm, and three are in the 0 to −20 ppm range. The eighth occurs at 2.3 ppm. This one is clearly observed in the T_1 inversion recovery spectrum shown in inset B. This spectrum also allows the three methyl resonances to be distinguished. One of these, that at lowest field, has twice the intensity of the other two. The spectrum is consistent with the presence of a five-coordinate complex in solution. The observation of eight methylene resonances indicates that each of the diastereotopic methylene protons is in a unique environment. There is a noticeable variation in line widths for the methylene protons with those that experience an upfield hyperfine shift displaying broader resonances (and thus appearing shorter in Figure 2). The following T_1 values have been measured, 11.9, 13.9, 11.3, and 13.5 ms for the four resonances between 65.5 and 55 ppm and 7.1, 6.2, and 5.3 ms for the three resonances between −3 and −21 ppm. These effects are remarkable since the methylene protons are all nearly equidistant from the iron and should have similar T_1 values and line widths if dipolar relaxation from a single center (the iron) dominates the relaxation process. The effect of temperature on the ^1H NMR spectrum is seen in the Curie plot in Figure 3. The methylene and meso resonances show linear behavior over the limited temperature range that was examined, but the extrapolated chemical shifts at $1/T = 0$ are far from the anticipated positions for a diamagnetic oxophlorin complex. Table I also contains data obtained for $ClFe^{III}(OEPO^{\cdot})$ which was prepared by the careful addition of a chloroform solution of dichlorine to **1**. The fact that distinct spectra with a common pattern and eight methylene resonances are seen for these two oxidation products indicates that, in solution, the halide ions remain coordinated to the iron center.

In order to have further insight into the unusual ^1H NMR spectrum of **2**, the corresponding complex **2a** (that is derived from etioporphyrin I) has been prepared by the addition of dibromine to $[Fe^{III}(\text{Etio I O})]_2$.[10] The ^1H NMR results are presented in Table I. The most significant features of the spectrum are the positions of the four pyrrole methyl resonances. Two are found with downfield hyperfine shifts (at 95.2 and 94.1 ppm) and two with upfield hyperfine shifts (at −14.7 and −51.9 ppm). Thus, two pyrrole rings have a spin density that is opposite to that on the other two pyrrole rings. As expected, the pyrrole methyl groups experience larger hyperfine shifts than do the corresponding methylene groups.

In chloroform solution at 296 K, the magnetic moment of $BrFe^{III}(OEPO^{\cdot})$ is 4.9(2) μ_B. The infrared spectrum for $BrFe^{III}(OEPO^{\cdot})$ is recorded in the Experimental Section. As expected, no O–H stretch is observed. The 1650–1500-cm^{-1} region is complex with four bands present. This is typical for other oxophlorin radical complexes (*e.g.*, $(py)Zn^{II}(OEPO^{\cdot})$[34] and $(py)_2Ni^{II}(OEPO^{\cdot})$[35]). For $BrFe^{III}(OEPO^{\cdot})$, no EPR spectrum was observed for a frozen dichloromethane solution of the complex at 6 K.

Crystal and Molecular Structure of $BrFe^{III}(OEPO^{\cdot})CHCl_3$. The structure of this oxidized complex has been determined by X-ray crystallography. The asymmetric unit consists of one complex molecule and one molecule of chloroform. There is no crystallographically imposed symmetry on either molecule. A drawing of both molecules is shown in Figure 4. Selected bond distances are given in Table II. Table III gives a selection of significant bond angles.

The iron is five-coordinate with bonds of nearly equal length (avg Fe–N, 2.066 Å) to the four pyrrole nitrogen atoms. The Fe–N distances all fall within the range (2.060–2.087 Å) that

(39) If the dipolar contribution to the line widths from the iron dominates the relaxation, then the line widths should be proportional to r^{-6}, where r is the distance from the proton of interest to the iron. Thus, line widths should increase in the order methyl, methylene, meso.[40]

(40) Swift, T. J. In *NMR of Paramagnetic Molecules*; La Mar, G. N., Horrocks, W. D., Jr., Holm, R. H., Eds.; Academic Press: New York, 1973; p 53.

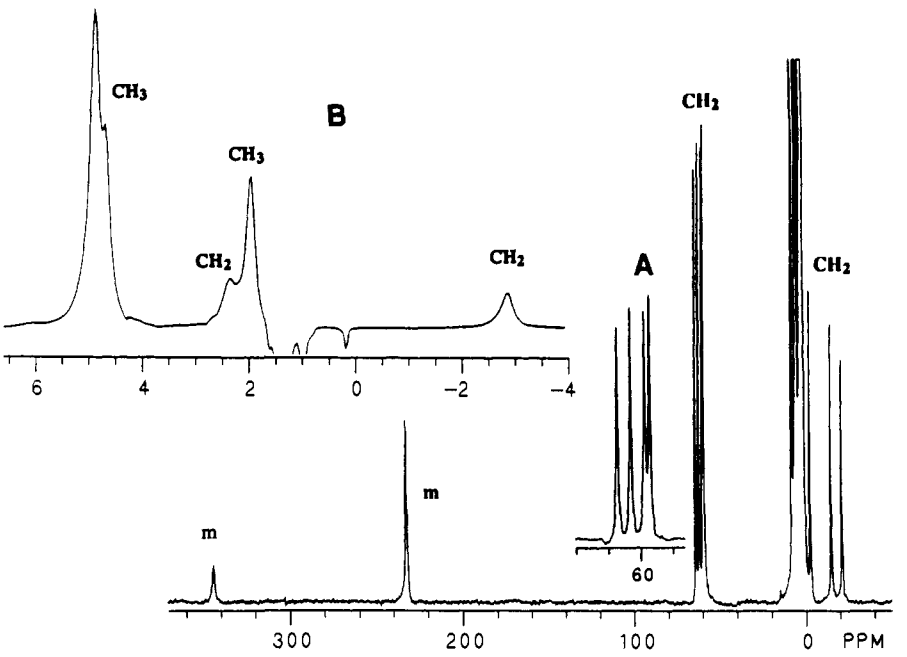

Figure 2. 300-MHz ^{1}H NMR spectrum of BrFe^{III}(OEPO$^{\cdot}$) in chloroform-*d* at 24 °C. Inset A shows an expansion of the methylene resonances at *ca.* 60 ppm. Inset B shows the 8 to −4 ppm regions under T_1 inversion recovery conditions where the resonances of diamagnetic material appear inverted.

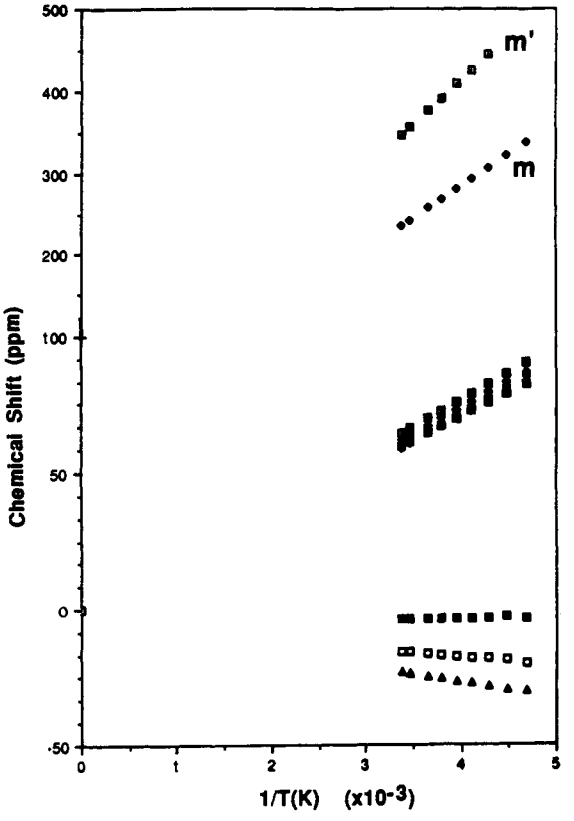

Figure 3. Plot of the chemical shifts for the methylene and meso (m, m') protons of BrFe^{III}(OEPO$^{\cdot}$) in chloroform-*d* versus $1/T$.

has been observed for high-spin ($S = {}^5/_2$), five-coordinate iron porphyrins. The Fe–Br distance is 2.367(2) Å, which is slightly longer than the corresponding distance (2.348(2) Å) in BrFe^{III}(TPP).

The macrocycle is ordered. That is unusual for a complex derived from octaethyloxophlorin. Previous structural work on zinc(II) and nickel(II) complexes of the octaethyloxophlorin radical dianion showed disorder in the position of the meso oxygen.[35,36] In BrFe^{III}(OEPO$^{\cdot}$), however, this meso substituent is well behaved. This can be attributed to the interaction with

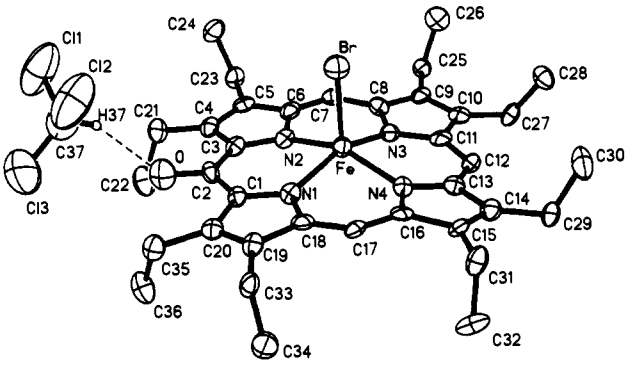

Figure 4. Perspective view of BrFe^{III}(OEPO$^{\cdot}$) showing 50% thermal contours. The hydrogen bond from chloroform to the meso keto oxygen is shown as a dashed line.

Table II. Selected Bond Lengths (Å) for BrFe^{III}(OEPO$^{\cdot}$)CHCl$_3$

Fe–Br	2.367(2)	Fe–N(1)	2.073(8)
Fe–N(2)	2.070(9)	Fe–N(3)	2.068(9)
Fe–N(4)	2.054(8)	O–C(2)	1.250(14)
N(1)–C(1)	1.366(13)	N(1)–C(18)	1.407(13)
N(2)–C(3)	1.353(14)	N(2)–C(6)	1.409(13)
N(3)–C(8)	1.385(13)	N(3)–C(11)	1.386(14)
N(4)–C(13)	1.363(14)	N(4)–C(16)	1.424(12)
C(1)–C(2)	1.434(14)	C(1)–C(20)	1.435(14)
C(2)–C(3)	1.445(14)	C(3)–C(4)	1.432(14)
C(4)–C(5)	1.376(15)	C(5)–C(6)	1.450(15)
C(6)–C(7)	1.365(15)	C(7)–C(8)	1.387(15)
C(8)–C(9)	1.437(15)	C(9)–C(10)	1.374(15)
C(10)–C(11)	1.442(15)	C(11)–C(12)	1.403(14)
C(12)–C(13)	1.400(14)	C(13)–C(14)	1.457(14)
C(14)–C(15)	1.358(16)	C(15)–C(16)	1.468(15)
C(16)–C(17)	1.346(15)	C(17)–C(18)	1.380(15)
C(18)–C(19)	1.435(15)	C(19)–C(20)	1.361(15)

a chloroform molecule which acts as a hydrogen-bond donor. The O···HCCl$_3$ distance is 2.096 Å, which is consistent with the presence of a hydrogen bond. The O–C(2) distance (1.250(14) Å) is in the range expected for a carbon–oxygen double bond. This suggests that there is significant keto character to this meso substituent.

The macrocycle is not completely planar as the diagram in Figure 5 shows. There is a slight, saddle-shaped distortion with

Table III. Selected Bond Angles (deg) for $BrFe^{III}(OEPO^{\cdot})CHCl_3$

Br–Fe–N(1)	100.0(3)	Br–Fe–N(2)	101.7(3)
N(1)–Fe–N(2)	86.7(3)	Br–Fe–N(3)	105.9(3)
N(1)–Fe–N(3)	154.1(4)	N(2)–Fe–N(3)	87.4(3)
Br–Fe–N(4)	104.0(3)	N(1)–Fe–N(4)	88.0(3)
N(2)–Fe–N(4)	154.3(4)	N(3)–Fe–N(4)	86.6(3)
Fe–N(1)–C(1)	128.9(6)	Fe–N(1)–C(18)	124.5(7)
C(1)–N(1)–C(18)	105.5(8)	Fe–N(2)–C(3)	129.0(7)
Fe–N(2)–C(6)	123.3(7)	C(3)–N(2)–C(6)	105.6(8)
Fe–N(3)–C(8)	126.4(7)	Fe–N(3)–C(11)	127.9(7)
C(8)–N(3)–C(11)	104.1(8)	Fe–N(4)–C(13)	129.2(6)
Fe–N(4)–C(16)	124.2(7)	C(13)–N(4)–C(16)	104.9(8)
N(1)–C(1)–C(2)	123.8(9)	N(1)–C(1)–C(20)	110.8(8)
C(2)–C(1)–C(20)	125.4(9)	O–C(2)–C(1)	117.5(9)
O–C(2)–C(3)	117.9(9)	C(1)–C(2)–C(3)	124.5(10)
N(2)–C(3)–C(2)	123.9(9)	N(2)–C(3)–C(4)	112.4(9)
C(2)–C(3)–C(4)	123.7(10)	C(3)–C(4)–C(5)	105.7(9)
C(4)–C(5)–C(6)	107.5(9)	N(2)–C(6)–C(5)	108.7(9)
N(2)–C(6)–C(7)	125.1(10)	C(5)–C(6)–C(7)	126.0(9)
C(6)–C(7)–C(8)	128.4(9)	N(3)–C(8)–C(7)	122.1(9)
N(3)–C(8)–C(9)	111.3(9)	C(7)–C(8)–C(9)	126.5(9)
C(8)–C(9)–C(10)	107.1(9)	C(9)–C(10)–C(11)	105.6(10)
N(3)–C(11)–C(10)	111.9(9)	N(3)–C(11)–C(12)	124.4(9)
C(10)–C(11)–C(12)	123.7(10)	C(11)–C(12)–C(13)	125.3(10)
N(4)–C(13)–C(12)	124.3(9)	N(4)–C(13)–C(14)	112.7(9)
C(12)–C(13)–C(14)	122.9(10)	C(13)–C(14)–C(15)	105.5(9)
C(14)–C(15)–C(16)	108.4(9)	N(4)–C(16)–C(15)	108.5(9)
N(4)–C(16)–C(17)	124.3(9)	C(15)–C(16)–C(17)	126.8(9)
C(16)–C(17)–C(18)	127.8(10)	N(1)–C(18)–C(17)	124.7(10)
N(1)–C(18)–C(19)	109.3(9)	C(17)–C(18)–C(19)	126.0(9)
C(18)–C(19)–C(20)	107.4(9)		

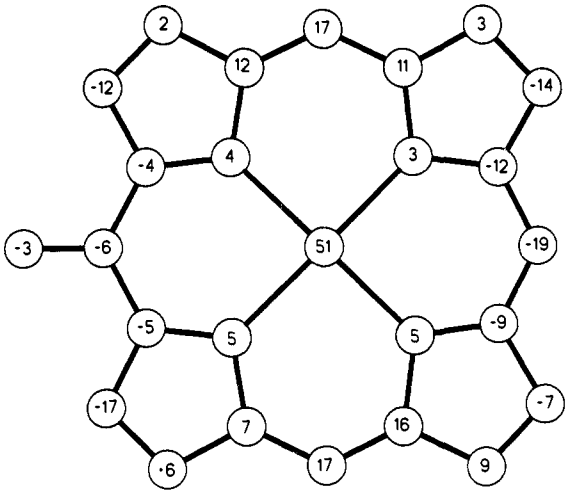

Figure 5. Diagram of the macrocyclic core of $BrFe^{III}(OEPO^{\cdot})$. Each atom symbol has been replaced by a number that represents the perpendicular displacement (in units of 0.01 A) of that atom from the mean plane of the macrocycle.

two of the meso carbons bent down and two bent up. The iron lies 0.50 Å out of the mean plane of the macrocycle and 0.46 Å out of the N_4 plane. These displacements are consistent with observations on five-coordinate, high-spin iron(III) porphyrins. For these, displacements of iron from the porphyrin plane of 0.39–0.62 Å and from the N_4 plane of 0.39–0.54 Å are found.[41]

In the solid, pairs of $BrFe^{III}(OEPO^{\cdot})$ molecules are positioned about centers of symmetry so that there is face-to-face, π–π contact. The two molecules do not fully overlay one another as seen for $[(H_2O)Zn(OEP^{\cdot})]_2ClO_4$,[42,43] $[Ni(OEP^{\cdot})]_2(ClO_4)_2$, or $[Fe(OEP^{\cdot})Cl]_2(ClO_4)_2$.[44] Rather, they are offset as is commonly

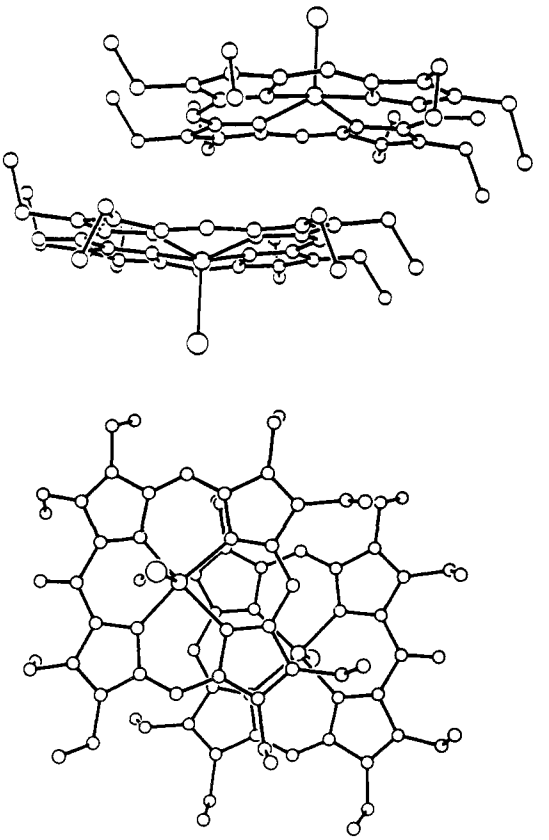

Figure 6. Views of a pair of $BrFe^{III}(OEPO^{\cdot})$ molecules showing the overlap between adjacent molecules in the solid.

seen when porphyrin macrocycles stack over one another.[45] This offset is best seen by referring to Figure 6, which shows two views of the pair of molecules. The lower view is oriented so that one looks down upon two nearly parallel molecular planes. Within this pair, the mean plane separation is 3.52 Å and the lateral shift of the oxophlorin centers is 3.55 Å. The distance from one oxophlorin center to the other is 5.00 Å, and the iron–iron separation is 5.77 Å. The shortest C···C contact within this pair is 3.623 Å. It involves C(7) and C(13a). The lateral shift and the mean plane separation within **2** place this molecule in group I of the classification of Scheidt and Lee.[45] This is the group with an intermediate degree of π···π overlap.

It is interesting to note, however, that despite the close approach of the two molecules within this pair, the closest intermolecular C···C contact does not involve this pair. Rather, the nearest C···C contact occurs with yet another molecule, one that shows little direct π–π overlap. This is illustrated in Figure 7. In this stereoview, the shortest C···C separation (3.352 Å) involves the two meso carbons which are found in the pair shown on the left side. In this context, it is interesting to notice that the dimerization of $Ni(OEPO^{\cdot})$ occurs through the meso carbons.[37] However, in that case, the macrocycle undergoes a pronounced saddle-shaped distortion and a new carbon–carbon bond (bond length, 1.614(8) Å) is formed. The nonbonded C···C separation between carbons in Figure 7 is twice as long as that.

Spectroscopic Characterization of $Br_2Fe^{III}(OEPOx)$. Addition of 2 mol of dibromine to $[Fe^{III}(OEPO)]_2$ in a 2:1 molar ratio produces another red complex, $Br_2Fe^{III}(OEPOx)$, **3**, which can be isolated as fine red plates. Unfortunately, crystals of this compound that would be suitable for an X-ray diffraction study have not been obtained.

The electronic absorption spectrum of the complex is shown in trace B of Figure 1. An unusual three-band pattern is seen. This spectrum is not like the absorption spectra of iron complexes

(41) Scheidt, W. R.; Reed, C. A. *Chem. Rev.* **1981**, *81*, 543.
(42) Song, H.; Reed, C. A.; Scheidt, W. R. *J. Am. Chem. Soc.* **1989**, *111*, 6867.
(43) Song, H.; Orosz, R. D.; Reed, C. A.; Scheidt, W. R. *Inorg. Chem.* **1990**, *29*, 4274.
(44) Scheidt, W. R.; Song, H.; Haller, K. J.; Safo, M. K.; Orosz, R. D.; Reed, C. A.; Debrunner, P. G.; Schulz, C. E. *Inorg. Chem.* **1992**, *31*, 941.
(45) Scheidt, W. R.; Lee, Y. J. *Struct. Bonding (Berlin)* **1987**, *64*, 1.

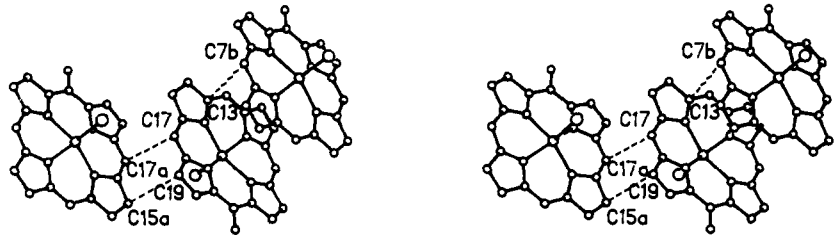

Figure 7. Stereoview showing the orientations of three molecules of $BrFe^{III}(OEPO^{\cdot})$ in the solid state. The pair shown in Figure 6 is on the right. The shortest nonbonded C···C contacts are C(17)···C(17a), 3.352 Å; C(7b)···C(13), 3.623 Å; and C(19)···C(15a), 3.629 Å.

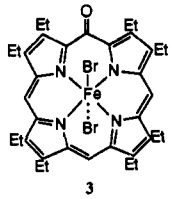

3

of porphyrins, oxophlorins, or oxophlorin radicals. Most notably, the intensities of the bands at 393 and 449 nm are weaker than those of the Soret bands of porphyrins, which typically have extinction coefficients of 10^5. This indicates that the electronic structure of the macrocycle in $Br_2Fe^{III}(OEPOx)$ is considerably altered from that of a porphyrin.

The ^1H NMR spectrum of $Br_2Fe^{III}(OEPOx)$ in chloroform-*d* at 24 °C is shown in Figure 8. This spectrum is considerably simpler than the one shown in Figure 2. There are four equally intense methylene resonances in the 60–30 ppm region. The meso protons produce broader resonances at 21 and 34 ppm in a 2:1 intensity ratio. The four resonances between 5 and 7 ppm (see inset A) are due to the four methyl groups in the complex. The overall pattern of the resonances is consistent with the presence of equivalent coordination of the iron on either side of the porphyrin plane, and is consistent with a six-coordinate structure with two axial bromide ligands. The temperature dependence of the ^1H NMR spectrum is presented in Figure 9. The plots for each functional group are linear, but the extrapolated positions at $1/T = 0$ are somewhat outside the range expected.

Figure 10 shows the electron-spin resonance spectrum that was obtained from a frozen dichloromethane solution of the complex at 6 K. The spectrum is characteristic of an axially symmetric complex with a high-spin ($S = {}^5/_2$) iron(III) ion. The hyperfine structure in the $g_\parallel$ feature at $g = 2.0$ is particularly informative. A septet with a 1:2:3:4:3:2:1 intensity ratio is clearly resolved. This is caused by coupling of the spin to two equivalent bromine nuclei (^{79}Br, 50.5%, and ^{81}Br, 49.5%, natural abundance; both spin $^3/_2$). The hyperfine coupling constant observed for bromine is 25 G, which is consistent with values seen in similar high-spin iron(III) complexes.[10,46]

The magnetic moment of $Br_2Fe^{III}(OEPOx)$ in the solid state is 5.8(1) μ_β. In chloroform solution at 25 °C, the magnetic moment is 5.7(2) μ_β. These, like the EPR results, indicate that the iron is in the high-spin ($S = {}^5/_2$) state.

The infrared spectrum for $Br_2Fe^{III}(OEPOx)$ is recorded in the Experimental Section. The band at 1734 cm^{-1} is probably due to the C–O stretch of the keto substituent. Notice that there are no bands in this region for either $[Fe^{III}(OEPO)]_2$ or $BrFe^{III}(OEPO^{\cdot})$.

Electronic Structure of the Oxophlorin Radical. Semiquantitative Fenske–Hall LCAO molecular orbital calculations[47] were performed on the oxophlorin trianion. The macrocyclic structure was assumed to be fully planar, and typical C–C, C–N, and C–O distances were used to maintain C_{2v} symmetry. Figure 11 shows the electron distribution in the highest occupied molecular orbital—this orbital will be singly occupied in the ligand radical. The calculations anticipate high spin density at the oxygen atom and the three other meso carbon atoms and preferential localization of spin density on two of the four pyrrole rings. These results are in substantial agreement with earlier calculations.[12]

Discussion

The results presented here show that the iron(III) oxophlorin dimer **1** undergoes two successive oxidations to produce the monomeric complexes **2** and **3**. In both cases, the axial Fe–O bonds of **1** are broken. The reaction stoichiometry determines which product is obtained. Both products are readily isolated, and both are stable to air. However, on prolonged storage, **3** is slowly converted back to **2**.

All available evidence indicates that these oxidations are predominantly ligand, rather than metal, centered. The ability of octaethyloxophlorin itself and metal complexes of this ligand such as (py)Zn(OEPOH···py) and Ni(OEPOH) to undergo one-electron oxidation is well established.[35,36] The observation of two successive one-electron oxidations for these iron complexes makes this a complete electron-transfer series.[48]

The fact that the ^1H NMR spectra of **2** and **3** do not show concentration effects indicates that these complexes do not aggregate in solution. This is particularly significant for the radical complex **2** which can be compared to a number of other radical complexes, especially $Ni^{II}(OEPO^{\cdot})$ which associates in solution[34] and dimerizes in the solid state.[13] Compound **3** remains monomeric both in solution and in the solid state, despite the fact that with only a five-coordinate iron, it possesses one exposed face. In the solid state, it also shows what must be considered a modest degree of overlap with adjacent molecules. In this context, it is important to realize that $[ClFe^{III}(OEP^{\cdot})]_2(ClO_4)_2$, $[(H_2O)Zn^{II}(OEP^{\cdot})]_2(ClO_4)_2$, and $[Ni^{II}(OEP^{\cdot})]_2(ClO_4)_2$ all crystallize as tight, cofacial pairs with strong interaction between constituents.[42-44] This is particularly apparent in $[(H_2O)Zn^{II}(OEP^{\cdot})]_2(ClO_4)_2$ where the face-to-face overlap produces a diamagnetic solid.

For **2**, there are several alternative electronic structures that need to be considered. Because of the ease of oxidation of the oxophlorin ligand, the $BrFe^{III}(OEPO^{\cdot})$ formulation is a natural possibility. However, formulation as an iron(IV) complex, $BrFe^{IV}(OEPO)$, with the ligand present as the OEPO trianion is also a reasonable possibility. The magnetic moment (4.9 μ_B at 298 K) presents certain limitations on these formulations. The magnetic moment could accommodate a high-spin ($S = 2$) Fe(IV) formulation. However, all previously characterized Fe(IV) porphyrin complexes have an intermediate spin ($S = 1$) ground state and a significantly lower magnetic moment.[14-16] For an Fe(III)/oxophlorin radical formulation, the identification of the electronic structure requires a description of the magnetic coupling between the two paramagnetic centers (ligand and metal). If the iron is present in the high-spin ($S = {}^5/_2$) state (and the structural data strongly support this assumption), then three limiting cases of magnetic coupling exist. If the two centers ($S = {}^5/_2$ and $^1/_2$) are noninteracting, then a magnetic moment of 6.17 μ_B is expected.

(46) Van Camp, H. L.; Scholes, C. P.; Mulks, C. F. *J. Am. Chem. Soc.* **1976**, *98*, 4094.
(47) Hall, M. B.; Fenske, R. F. *Inorg. Chem.* **1972**, *11*, 768.
(48) Balch, A. L.; Holm, R. H. *J. Am. Chem. Soc.* **1966**, *88*, 5201.

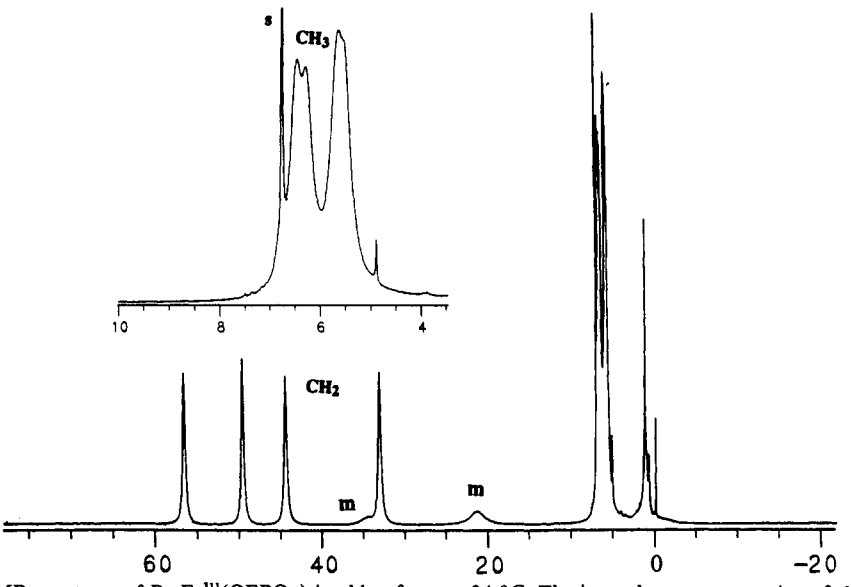

Figure 8. 300-MHz ^{1}H NMR spectrum of Br_2Fe^{III}(OEPOx) in chloroform at 24 °C. The inset shows an expansion of the 10–4 ppm region.

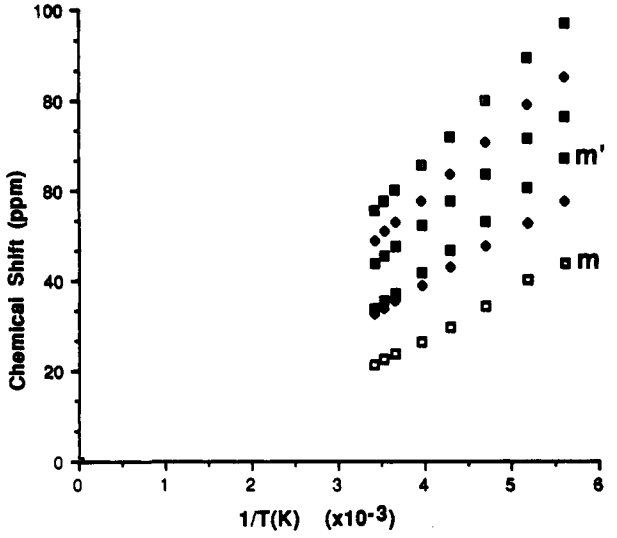

Figure 9. Plot of the chemical shifts for the methylene and meso (m, m′) resonances of Br_2Fe^{III}(OEPOx) versus $1/T$.

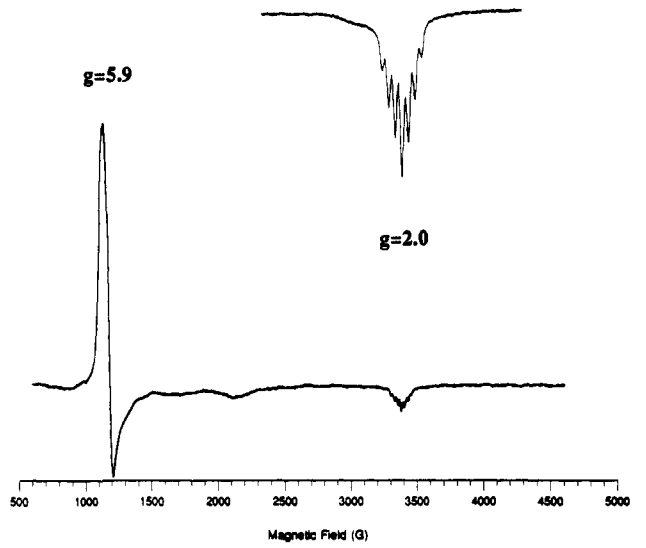

Figure 10. Electron-spin resonance spectrum of Br_2Fe^{III}(OEPOx) in frozen dichloromethane at 6 K.

If there is strong ferromagnetic coupling, the expected magnetic moment is 6.9 μ_B. However, with strong antiferromagnetic coupling between the iron and the ligand, a magnetic moment of 4.9 μ_B is anticipated.[22] The measured magnetic moment (4.9(2) μ_B) is clearly consistent with the last proposition, the existence of strong antiferromagnetic coupling between the ligand and the iron, and it is too small to allow for the existence of either noninteracting centers or ferromagnetically coupled centers. The low symmetry of complex **2** facilitates the antiferromagnetic coupling. In the idealized C_s symmetry of this five-coordinate complex, the five half-filled orbitals ($d_{x^2-y^2}$, d_{z^2}, $d_{xz}-d_{yz}$, $d_{xz}+d_{yz}$, d_{xy}) have a″, a′, a″, a′, and a′ symmetry, respectively. The symmetry of the half-filled oxophlorin orbital (Figure 11) is a′; thus, the overlap of this orbital with three of the metal orbitals becomes allowed. Thus, there is no symmetry barrier to antiferromagnetic coupling. Likewise, the factors that favor ferromagnetic coupling in higher symmetry porphyrin complexes[23] are absent in **2**.

The ^{1}H NMR spectral data for $BrFe^{III}$(OEPO·) show a number of remarkable features that must arise from its unusual electronic structure but which can be understood in the context of the nature of the half-filled molecular orbital (Figure 11) and the antiferromagnetic coupling. The observed pattern for high-spin (OEP)-$Fe^{III}X$ gives the meso protons upfield hyperfine shifts and the

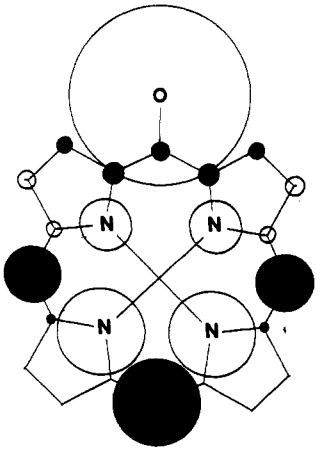

Figure 11. Representation of the electron density and the phases of the highest occupied π-molecular orbital for the oxophlorin trianion.

methylene protons downfield shifts as a result of the σ and π contributions from the iron spins to the electronic structure.[10] However, the presence of the unpaired spin in the ligand radical dominates the hyperfine shifts in $BrFe^{III}$(OEPO). The meso

resonances have strikingly large, downfield hyperfine shifts. Normally, unpaired spin density in the π-ligand orbital would be expected to produce upfield shifts for the meso protons with the m′ proton expected to show the largest shift.[12] However, the presence of antiferromagnetic coupling alters the situation.[49] The high-spin iron center is aligned with the magnetic field, and the antiferromagnetic coupling to the ligand π-radical reverses the spin orientation within the ligand. Consequently, large downfield shifts are observed with the m′ proton expected to show the largest shift, as it does. The methylene resonances are divided into two distinct sets. Four methylene resonances have downfield shifts while four other display upfield shifts. Similarly for $BrFe^{III}$(Etio I O·), two pyrrole methyl groups display downfield hyperfine shifts while two others show upfield shifts. Thus, the available data indicate that the signs of the spin densities on two pyrrole rings are opposite those on the other two pyrrole rings. The occurrence of this peculiar pattern for a ligand π-radical can only be explained if there is antiferromagnetic coupling between the two paramagnetic centers (iron and ligand radical) and therefore the opportunity for each to contribute to the spin distribution within the individual pyrrole rings. The data in Figure 3 show that the temperature dependence of the ^{1}H NMR spectra of $BrFe^{III}$(OEPO·) has interesting behavior. The plots are linear, but the extrapolated chemical shifts at $1/T = 0$ are far removed from the shifts expected on the basis of observations of diamagnetic oxophlorin and porphyrin complexes. This atypical behavior can be a result of thermal effects on the antiferromagnetic coupling between the ligand and metal spins and/or the thermal equilibrium between different orbital states for the radical. Finally, the ^{1}H NMR spectrum of $BrFe^{III}$(OEPO·) shows an unusual distribution of T_1 values for the methylene protons. Those with downfield shifts have T_1 values that are approximately double those of the methylene protons with upfield shifts. Since these protons are all nearly equidistant from the iron, they should experience similar dipolar relaxation. A scalar mechanism for relaxation should produce a reversed order of T_1 values. The variation seen can be explained by the presence of a second paramagnetic center, the ligand radical, which causes differential relaxation that depends on the spin distribution within the ligand π framework.

For **3**, the formulation as a high-spin ($S = {}^5/_2$) iron(III) complex is supported by the magnetic moment (5.8(2) μ_B) and by the characteristic EPR spectrum shown in Figure 10. These data require then that the ligand has undergone oxidation, and the observation of a ketonic feature at 1734 cm^{-1} in the infrared spectrum is certainly consistent with ligand-based oxidation. Now, since **3**, which is more highly oxidized than **2**, contains iron(III), it is also reasonable that **2**, which involves a less-oxidizing ligand, also contains iron in the same oxidation state. The ^{1}H NMR spectral pattern seen for Br_2Fe^{III}(OEPOx) is fairly typical of those seen for six-coordinate, high-spin iron(III) porphyrins and related complexes. These typically show downfield shifts for both the methylene and meso resonances.[50-53] The downfield meso shifts have been used as an empirical indicator of six-coordination for iron(III) porphyrins.

Further work is necessary to establish whether the oxidation products **2** and **3** or the derivatives of these which might differ in their axial ligation are involved in either the coupled oxidation process or the mechanism of action of heme oxygenase. From the present work, however, it is clear that any species analogous to **2** should be readily detectable through ^{1}H NMR studies because of the very large and characteristic downfield hyperfine shifts of the meso proton resonances. It will be interesting to determine what effect changes in the axial ligation and the protonation state of the meso keto substituent have on the magnetic properties. Nevertheless, it is clear from the present study that ligand-centered oxidations occur in these complexes and that $BrFe^{III}$(OEPO·) possesses a remarkable electronic structure.

Table IV. Crystallographic Data for $BrFe^{III}$(OEPO·)$CHCl_3$

formula	$C_{37}H_{44}BrCl_3FeN_4O$
fw	802.9
color and habit	dark red plate
crystal system	triclinic
space group	$P\bar{1}$
a (Å)	10.379(2)
b (Å)	12.283(3)
c (Å)	14.681(3)
α (deg)	90.70(2)
β (deg)	89.83(2)
γ (deg)	99.79(2)
V (Å^3)	1844.1(7)
T (K)	127
Z	2
d_{calcd} (mg m^{-3})	1.446
radiation (Å)	Cu Kα (λ = 1.54178 Å) (Ni filter)
μ(Cu Kα) (mm^{-1})	6.819
range of trans factors	0.56–0.94
no. data collected	4814
no. unique data	4505 (R_{int} = 0.034)
no. data refined	3063 ($F > 6.0\sigma(F)$)
no. parameters refined	423
R^a	0.084
$R_w{}^a$	0.098

^{a} $R = \sum||F_o| - |F_c||/|F_o|$ and $R_w = \sum||F_o| - |F_c|w^{1/2}/\sum|F_o w^{1/2}|$.

Experimental Section

Preparation of Compounds. Octaethyloxophlorin,[54] $[Fe^{III}(OEPO)]_2$,[10] and $[Fe^{III}$(Etio I O)$]_2$[10] were prepared by known routes.

$BrFe^{III}$(OEPO·). A solution of bromine in chloroform (0.85 μL of a 9.71 M solution) was added to a solution of 10 mg (8.3×10^{-3} mmol) of $[Fe^{III}(OEPO)]_2$ in 5 mL of chloroform. The bright red solution was evaporated to dryness. The red solid was recrystallized from chloroform/hexane to yield the product as red crystals; yield 11.3 mg, 93%. IR (mineral oil mull): 1618, 1592, 1562, 1537, 1273, 1255, 1226, 1176, 1114, 1075, 1065, 1056, 1019, 1002, 956, 912, 865, 737, 695 cm^{-1}.

Br_2Fe^{III}(OEPOx). A solution of bromine in chloroform (1.7 μL of a 9.71 M solution) was added to 10 mg (8.3×10^{-3} mmol) of $[Fe^{III}(OEPO)]_2$ in 5 mL of chloroform. The solution was evaporated to dryness. The product was recrystallized from dichloromethane/*n*-hexane; yield 12.7 mg, 67%. IR: 1734, 1632, 1592, 1545, 1301, 1275, 1235, 1205, 1163, 1149, 1128, 1115, 1069, 1023, 987, 946, 912, 851, 828, 796, 760, 653 cm^{-1}. Anal. Calcd for $Br_2Fe^{III}(OEPOx)\cdot 0.25CH_2Cl_2$, $C_{36.25}H_{40.5}Br_2Cl_{0.5}FeN_4O$: C, 55.70; H, 5.22; N, 7.17; total halogen, 22.71. Found: C, 55.46; H, 5.68; N, 6.86; total halogen, 22.63. The presence of dichloromethane in the solid was verified by observing the ^{1}H NMR spectrum of the complex dissolved in chloroform-*d*.

X-ray Data Collection. A dark red plate of $BrFe^{III}$(OEPO·)$CHCH_3$ was obtained by diffusion of hexane into a chloroform solution of the complex. A suitable crystal was coated with a light hydrocarbon oil and mounted in the 130 K dinitrogen stream of a Siemens P4/RA diffractometer equipped with a locally modified low-temperature apparatus. A triclinic unit cell was obtained by indexing reflections from a rotation photograph and verified by examination of axial photographs. Two check reflections showed only random (<2%) variations in intensity during data collection. The data were corrected for Lorentz and polarization effects. Crystal data are collected in Table IV.

Solution and Structure Refinement. Calculations were performed on a DEC VAX station 3200 with SHELXTL Plus version 4.00. Scattering factors and corrections for anomalous dispersion were taken from a

(49) Banci, L.; Bertini, I.; Luchinat, C. *Struct. Bonding (Berlin)* **1990**, *72*, 113.
(50) Balch, A. L.; Olmstead, M. M.; Safari, N. *Inorg. Chem.* **1993**, *32*, 291.
(51) Budd, D. L.; LaMar, G. N.; Langry, K. C.; Smith, K. M.; Mayyir-Mazhir, R. *J. Am. Chem. Soc.* **1979**, *101*, 6091.
(52) Morishima, I.; Shiro, Y.; Walcino, T. *J. Am. Chem. Soc.* **1985**, *107*, 1063.
(53) Rajarathnam, K.; LaMar, G. N.; Chiu, M. L.; Sligar, S. G.; Singh, J. P.; Smith, K. M. *J. Am. Chem. Soc.* **1991**, *113*, 7886.
(54) Barnett, G. H.; Hudson, M. F.; McCombie, S. W.; Smith, K. M. *J. Chem. Soc., Perkin Trans. 1* **1973**, 691.

standard source.[55] The solution was determined by direct methods. Hydrogen atoms were treated by use of a riding model with a fixed isotropic *U*. An absorption correction was applied.[56] All non-hydrogen atoms were assigned anisotropic thermal parameters. The largest peak in the final difference map was 1.64 e $Å^{-3}$.

Instrumentation. ^1H NMR spectra were recorded on a General Electric QE-300 FT NMR spectrometer operating in the quadrature mode (^1H NMR frequency was 300 MHz). The spectra were collected over a 50-KHz bandwidth with 16 K data points and a 50-μs 45° pulse. For a typical spectrum, between 1000 and 5000 transients were accumulated with a 50-ms delay time. The signal to noise ratio was improved by apodization of the free inducting decay. Electronic spectra were obtained using a Hewlett-Packard diode array spectrometer. EPR spectra were obtained using a Brucker spectrometer operating at X-band.

Acknowledgment. We thank the NIH (GM-26226) for financial support.

Supplementary Material Available: Tables of atomic positional parameters, bond distances, bond angles, anisotropic thermal parameters, and crystal data for $BrFe^{III}(OEPO^{\cdot})CHCl_3$ (8 pages); listings of observed and calculated structure factors (17 pages). This material is contained in many libraries on microfiche, immediately follows this article in the microfilm version of the journal, and can be ordered from the ACS; see any current masthead page for ordering information.

(55) *International Tables for X-ray Crystallography*; Kynoch Press: Birmingham, England, 1974; Vol. 4.

(56) The method obtains an empirical absorption tensor from an expression relating F_o and F_c. Moezzi, B. Ph.D. Thesis, University of California, Davis, CA, 1987.